Sinkhole and soil-structure interactions: Development of an experimental model

Matthieu Caudron, Fabrice Emeriault, Richard Kastner, Marwan Al Heib

Sinkhole and soil-structure interactions: Development of an experimental model.

M. Caudron, F. Emeriault & R. Kastner
URGC Géotechnique, INSA de Lyon, VILLEURBANNE France

M. Al Heib
INERIS - LAEGO, Parc de Saurupt, NANCY FRANCE

ABSTRACT: Soil-structure interactions during a sinkhole phenomenon are analyzed with a physical small-scale model developed using an analogical two-dimensional soil and a building model. A test bed allowing fully controlled test is used. The paper presents the results of a series of tests during which vertical and horizontal displacements of the Schneebeli steel rods are determined with the Digital Image Correlation technique at different steps of the creation of an underground cavity. First, repeatability tests are performed as well as a greenfield test. Then the same initial conditions are considered for a test with a model of building located at ground level and above the cavity.

1 INTRODUCTION

Subsidence is the result of collapse of natural and man-made cavities induces damage on the buildings. Nevertheless the complex soil-structure interactions occurring during a sinkhole phenomenon are not well understood. The current procedure used to evaluate potential damage to buildings standing above a future sinkhole is to determine the soil movement in greenfield conditions and then to apply these movements to the structure, neglecting the possible interactions: see for example Deck et al. 2003.

The main purpose is to develop a small-scale experimental model using Schneebeli metallic rods that will allow highlighting the soil-structure interactions during such phenomenon. This analogical material was developed several year ago but it is still used in recent works: Dolzhenko et al. 2001 and Shashin et al. 2004. However, the results will not be quantitative but only qualitative because of the disrespect of some laws of similarities. Moreover the occurrence of sinkholes appears very suddenly. Displacements reach the surface as soon as the failure occurs. It is so difficult to define a specific state for the beginning of the failure.

A well documented sinkhole (Vachat 1982) is taken as a representative example of the many sinkholes observed in Paris each year (IGC 1999). It has been induced by the collapse of an underground cavity presenting the usual dimensions of the Parisian quarries: 8 m in width, 2 m in height and a cover of 8 m (Figure 1).

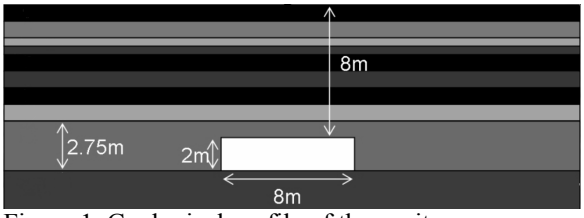

Figure 1. Geological profile of the cavity

Table 1. Soil properties of the documented sinkhole from laboratory tests (Vachat, 1982)

	Granular soil	Coherent soil
E (MPa)	50-100	50-100
ν	0.30	0.30
ρ (kg/m^3)	2200	2200
φ (°)	~26	~26
c (kPa)	0	200

Several soil layers compose the cavity cover. Their individual characteristics are presented in Fine 1993 but it can be roughly considered that they define two mechanical homogeneous layers: a 6 m thick cohesionless material overlying a 2 m thick cohesive layer whose mechanical characteristics are presented in Table 1. The building model is similar to a dwelling and comprises three spans and two stories. Its dimensions are 10 m in total width and each story in 2.7 m high (Figure 2). A crawl space is also represented. The small scale model dimensions are determined in order to satisfy the laws of similarity as accurately as possible.

2 THE LAWS OF SIMILARITIES

2.1 Assumptions

The assumption that the test will not depend on the thermal effect allows making the problem a bit sim-

pler: Dehousse & Arnould 1971 show that there are then nine equations controlling the scaling. Four of them are straightforward, the five remaining relations define the compatibility between the different scale factors. It appears that three scale factors can be chosen independently, the others then are deduced from the 5 compatibility equations.

2.2 The scale factors

The tests will be performed under normal gravity, the acceleration factor is thus 1. The analogical soil used has a unit weight of 65 kN/m^3. The corresponding scale factor can then be considered as equal to 3.

The scale factor on the lengths has been chosen as the last independent scale factor and in order to have a test bed with convenient dimensions, it has been fixed to 1/40. Therefore, it appears that the conversion of all the pressure type units to the small scale model must be done with a scale factor of 3/40 in order to meet the requirements of the laws of similarity.

2.3 The small-scale model

2.3.1 The analogical soils and the cavity

Using the different scale factors determined previously, the analogical soils should have a Young Modulus close to 4 up to 8 MPa. Neither their friction angles nor the Poisson coefficients are affected by the scale. The cohesion for the concerned layer should be around 15 kPa. The thickness of the two layers is 50 mm for the coherent one and 150 mm for the second one.

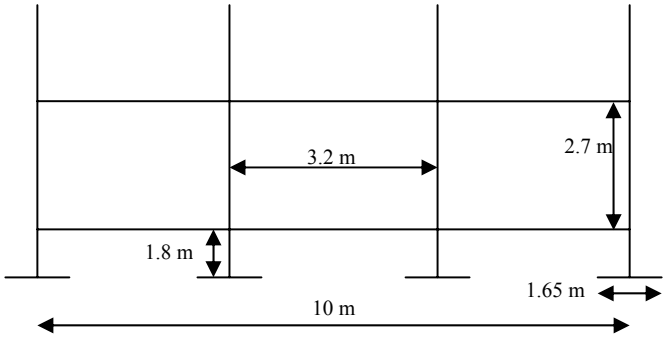

Figure 2. Dimensions of the real building.

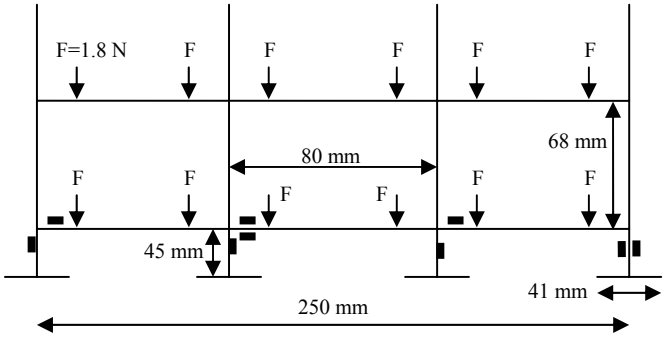

Figure 3. Dimensions and loading of the building model.

2.3.2 The building model

The geometry of the building model is shown on Figure 3. The thickness of the beams and the columns is 0.8 mm. This dimension allows having a building with a stiffness comparable with the stiffness of a real structure. Consequently, the weight of the building model is too small. Additional weights are placed on each of the horizontal beams to reach a total building weight compatible with the requirements of the laws of similarity.

3 THE EXPERIMENTAL MODEL

3.1 The test bed

The soil model has a maximum size of 750 mm width per 500 mm high above the cavity (corresponding to 30 m and 20 m respectively at full scale).

A small apparatus, inspired from the work of Nakai et al. 1997 focusing on tunneling induced soil movements, allows an easy and repetitive creation of the cavity. Moreover, cavities of different widths can be stepwise created: from 25 mm up to 250 mm in a maximum of 10 steps of 25 mm each. The height can also range from 25 to 100 mm but it has to be defined prior to the beginning of the test. At full scale, it corresponds to an opening of 1 to 10 m wide and 1 to 4 m high.

Ten moving parts of 25mm width numbered from 1 to 10 beginning at the left compose the total width of the cavity. Each one is equipped with a small force sensor on its top end. This will allow observing the variation of the forces applied by the soil mass to the remaining moving parts.

In order to follow the movements of the particles in the soil mass, a PIV-DIC procedure is used (Particle Image Velocimetry – Digital Image Correlation). White et al. 2003 clearly showed the pros and the cons of such method against photogrammetry. SIFASOFT, the software used to compute the displacements has been developed in LamCOS (INSA-LYON) by Touchal et al. 1997. The precision of the DIC method is around 1/100 pixel in very good conditions but with the presented apparatus and the corresponding test setup and procedure, the precision is only of 1/20 pixel. This corresponds to approximately 20 µm for a single couple of photos (0.8 mm at full scale). Therefore this value is sufficiently accurate for the purpose of this study.

3.2 The analogical soil

The basic analogical cohesionless soil is composed of metallic Schneebeli rods presenting three different diameters (3, 4 and 5 mm) for a length of 60 mm (see details in Dolzhenko et al. 2001).

In order to observe a sinkhole and not a subsidence trough, the underlying coherent soil layer

must be represented with the same assembly of metallic rods where cohesion is introduced. This is achieved by soaking the concerned rods in an aqueous solution of glue. Then these rods are manually put on the test bed in the desired place and dried until complete dehydration. The relative density can not be determined, but the basic property of this material is to present a constant porosity. The physical and mechanical characteristics of the cohesionless and coherent materials are presented in Table 2.

Table 2. Characteristics of the two materials

	Density	E (MPa)	φ (°)	c (kPa)
Cohesionless soil (prototype scale)	6.5	4-8	22-24	0
Full scale value	2.2	50-100	22-24	0
Coherent soil	6.5	4-8	27-30	~8
Full scale value	2.2	50-100	27-30	~100

3.3 The building models

The design of the building model was done assuming that it should stay in the elastic range whatever may be the foreseeable load.

The instrumentation of the structure model comprises 9 strain gauges and 4 displacement sensors (LVDT). The gauges are represented on Figure 3 by the black marks. The sensors are positioned on each foundation. They are all connected to a computer in order to log the different values at given times.

In Figure 3, the arrows represent the loading that are used during the test in order to have a convenient foundation loading.

4 THE RESULTS

4.1 The tests

Four different tests were performed. First, two identical tests were executed in order to analyse the repeatability of the procedure. Then a single test was conducted in greenfield conditions while the last test uses the same initial conditions but with the building model on the soil surface.

The two repeatability tests were done with the same conditions. The purpose was to test the measurement setup, to observe the mechanism of failure and several other parameters and then to compare them together. The geometrical parameters are 300 mm of total cover: with a 50 mm thick cohesive layer and a 250 mm thick granular soil layer. The cavity is 250 mm wide and 50 mm high.

For the greenfield test, only the total cover is different: 50 mm of cohesive material are still used but the granular soil is now 150 mm thick.

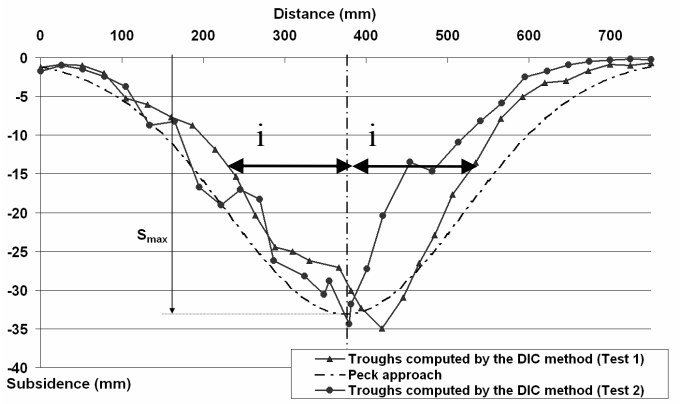

Figure 4. Subsidence troughs for the two repeatability tests and resulting from the empirical approach.

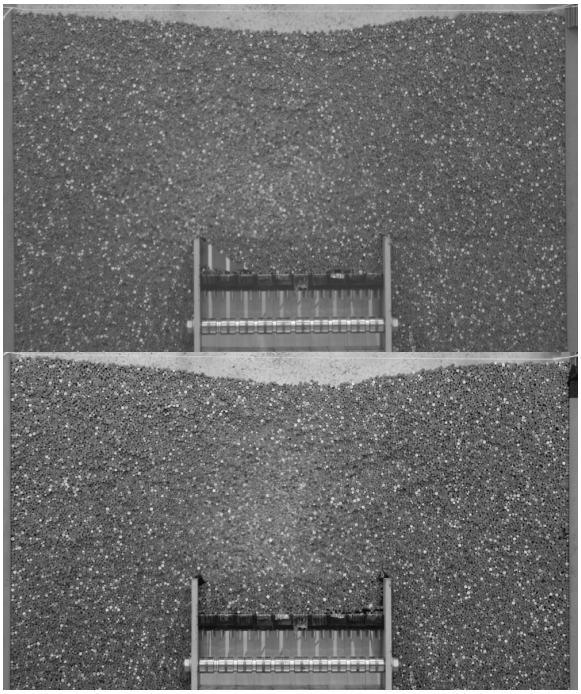

Figure 5. Failure mechanisms for the first test (up) and the second one (down).

The greenfield test is taken as a reference for the last test with the building model. The foundations are put under 15 mm of soil (60 cm in real scale, near the frost level). The left foundation of the building is located directly above the center of the cavity.

The procedure for each test comprises several steps necessary to obtain the complete failure of the cover. Digital photos, strains and displacements are logged at each step for further analysis.

The cavity is open in five steps (the parts 5 and 6 are lowered first, then 4 and 7 followed by 3 and 8 and so on), and then a stable state is reached. For the two repeatability tests, failure occurs during this last step. On the contrary, for the two other tests (Greenfield conditions and with the structure), it is necessary to weaken the cohesive layer by adding some water in the center of the cavity roof. This water is added in very small quantity. Photos and measures are logged each time when another degradation is applied.

4.2 *Comparisons and interpretations*

The two repeatability tests give similar results. Figure 4 shows the subsidence trough for each test when the failure of the cavity is complete. The maximum subsidence is respectively 33.2 mm and 31.6 mm (values computed by the DIC process). The distances to the point of inflection are very close: 140 mm and 150 mm. The volumes of the trough present only 7% of difference.

The empirical approach (after Peck) can be used to plot a theorical trough as shown by Caudron et al. 2003, using a circular equivalent cavity.

$$s_x = s_{\max} \times e^{\left(\frac{-x^2}{2i^2}\right)} \quad (1)$$

With s_x the vertical displacement, s_{max} the maximum vertical displacement, x the position to the center of the cavity and i the distance to the point of inflexion. The failure mechanisms are similar as shown on Figure 5. The only difference is located on the left part of the cavity, where a small void remains in the first test.

The horizontal displacements of the ground surface can be determined by the DIC method. They both are displayed on Figure 6 together with the theoretical shape on the movements plotted using the formula given by Lake et al. 1992.

$$v_x = s_x \frac{x}{z_0} \quad (2)$$

With z_0 the depth to the cavity axis and s_x the vertical displacement from the empirical approach (see Eq. 1). The maximal horizontal displacement predicted by Equation 2 is close to 14 mm while the computed ones for both tests are between 29 and 24 mm. The results are good for both tests in accordance with the theoretical shape, even though there may be some punctual differences.

During the tests, the forces on the cavity "pillars" are measured by the sensors placed on the moving pieces.

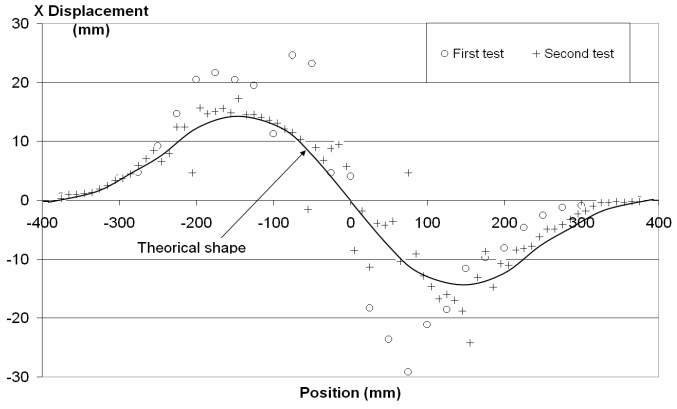

Figure 6. Horizontal displacements.

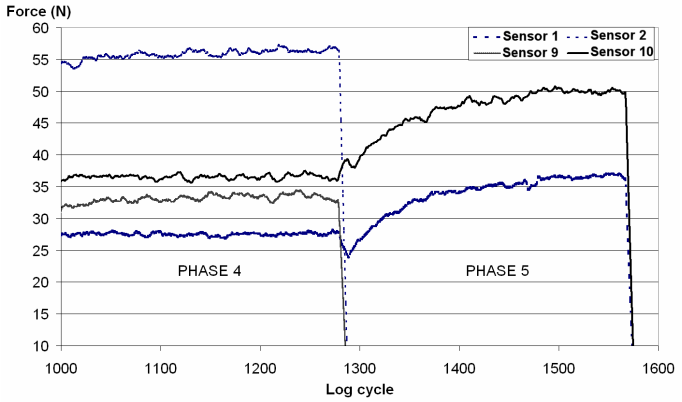

Figure 7. Transmission of the forces from the lowered parts to the adjacent remaining ones.

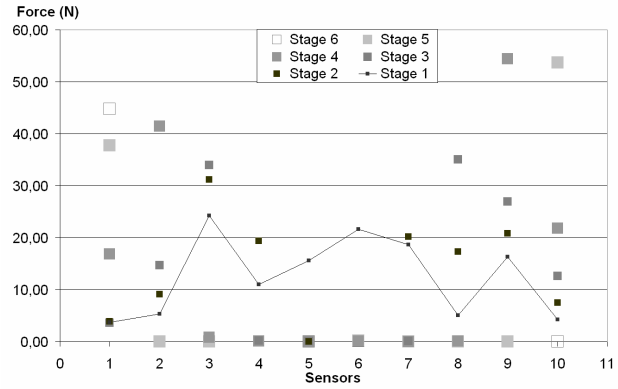

Figure 8. Evolution of the forces during the creation of the cavity (second test).

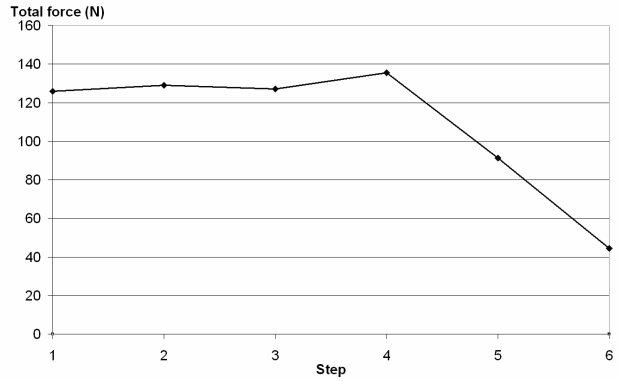

Figure 9. Variation of the total force measured by the force sensor.

Figure 7 illustrates the time-rate of the transmission of the load after the lowering of the two pieces. The phenomenon is not immediate; the transmission is gradual until reaching a state of balance with an increase close to 35% for each sensor. In the subsequent analysis, only the stable values obtained for each step are computed.

Figures 8 show the evolution of the forces acting on individual sensors during the second test. The gradual redistribution of the forces is clearly visible. Figure 9 represents the total force applied on the 10 sensors: the value is stable for the four first steps and then decreases during the two last steps. The weight of the soil mass is first totally transferred from the lowered pieces to the next ones and at the end of the creation of the cavity, part of this weight is transferred by arching effect directly to the soil mass.

4.2.1 Greenfield test

During the greenfield test, no significant movements on the ground surface can be observed before the weakening of the cohesive layer, even when the cavity is wide open. The maximum vertical movement measured by DIC is 0.2 mm. When water is gradually added, the occurrence of the sinkhole appears and the movements increase until the total failure of the cavity. One can notice on Figure 10 that the failure is not symmetric because of the right part of the cohesive layer still overhanging.

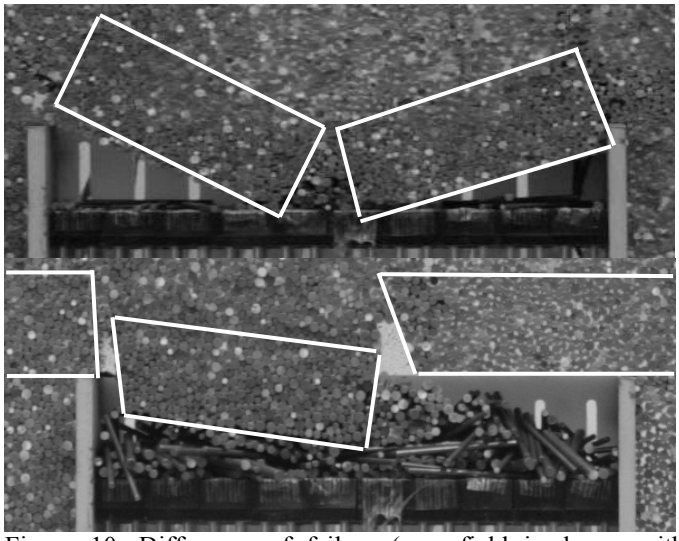

Figure 10. Difference of failure (greenfield is down, with structure is up).

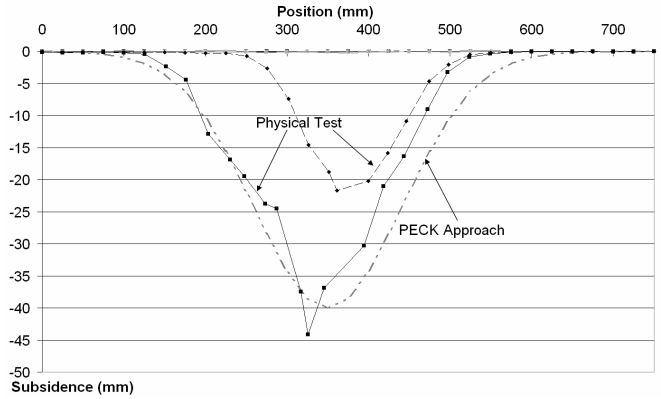

Figure 11. Subsidence troughs for the greenfield conditions. The two last stages are plotted where significant movements are observed.

Figure 11 shows the two main stages where noticeable subsidences reach the top of the soil mass.

The maximum settlement is approximately 44 mm (1.76 m at full scale). It is close to the height of the cavity (50 mm or 2 m at full scale). The width of the trough for the last step is 450 mm (18 m at full scale). As for the repeatability test, Peck's empirical approach can be used as presented by Caudron et al. 2003. The empirical curve is plotted on Figure 11. No important differences appear but on the right due to the partial failure of the cavity. It appears that the prediction of the soil subsidence in greenfield conditions is quite satisfying in spite of the difference of failure.

In the analysis of the horizontal displacements, two main states have to be considered: the first one when the failure is still symmetric (beginning of the sinkhole phenomenon), the second one when the left part of the cohesive layer falls into the cavity. Figure 12 illustrates the difference between the two cases: for the first one, the horizontal displacements present a similar shape to those seen during the repeatability tests whereas for the second one, the movement is completely located on the left part of the model (where the second failure appears). The shape is very different and oriented mainly towards the left.

4.2.2 Soil-structure interactions

The second test with the building model on the soil mass allows characterizing the soil-structure interactions. Figure 13 shows the final subsidence trough, compared with the greenfield results. The maximum vertical movement is 28% smaller than with the building. On the contrary, the width of the concerned area is 26% larger. But the volume of the trough is similar for both tests: respectively 443 cm^3 in greenfield and 481 cm^3 with the structure.

The horizontal displacement can be computed and compared to the results of the greenfield test. Figure 14 shows totally different behavior of the model, in shape and amplitude.

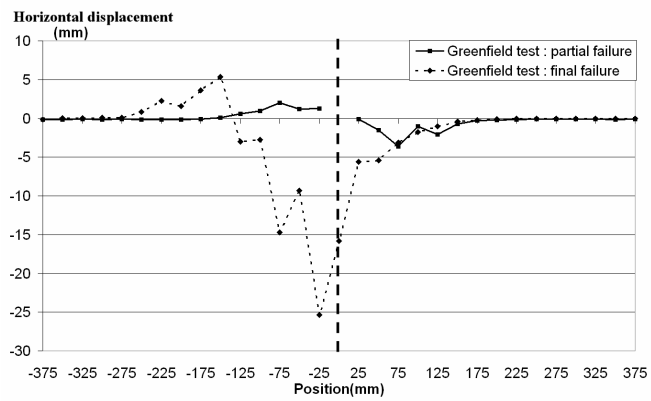

Figure 12. Horizontal displacement for the greenfield test.

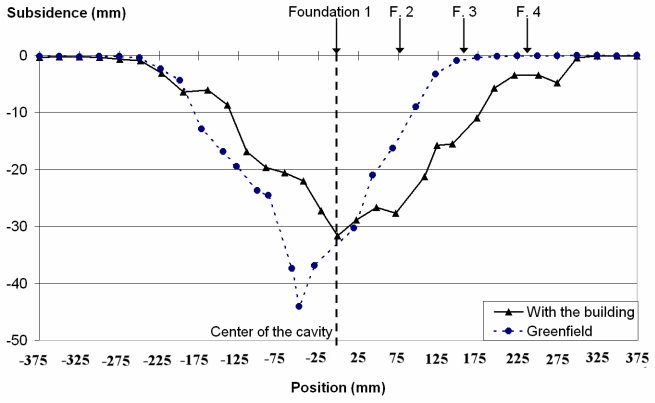

Figure 13. Comparison of the subsidence between the tests in greenfield and with the building model (the arrows represent the position of the four foundations).

Table 3. Comparison of the slopes for the three different spans named by the number of the two foundations delimiting them.

Span n°	Slope in green field	Slope with SSI
1-2	24.7%	5.1%
2-3	23.5%	17.9%
3-4	1.2%	12.3%

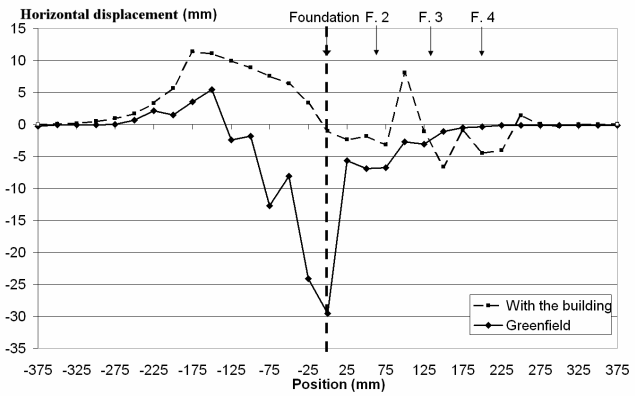

Figure 14. Horizontal displacement for the test with the building.

The last point, but not the less important, is the maximum slope. The difference between the two tests is important: 24.7% for the greenfield test and 17.9% with the building. Even though in both cases it would be very damageable for a building, these tests show that it could be very cost effective to consider the soil-structure interactions when studying the effect of a sinkhole or similar phenomenon on a building. If the relative settlements are more finely observed, it appears that the deformations in the structure are very different as shown in Table 3.

The approach commonly employed (the displacement in greenfield are applied directly on the building) would consider too large deformations and moreover in the wrong part of the building compared to the results given by the soil-structure interactions approach.

4.3 Improvements

Even though the results obtained in this study are interesting and convincing, some improvements need to be done in the future. The results from the small scale building instrumentation can not for now be used to understand the effect of the soil-structure interactions on the building. The dynamic effect need to be more finely observed by the use of a high-speed camera.

5 CONCLUSION

In conclusion, it appears that physical model presents some results in good accordance with the empirical methods. Moreover the soil-structure interactions observed when the building is used are obvious. Even though the modifications are not on the volume of the subsidence trough but on its shape which becomes very asymmetrical.

The design of this experimental model allowing the study of soil-structure interaction is the first step in a larger research project. Now that the small scale model is ready and only need some improvements, some parametric studies can be considered such as the cavity geometry, the position of the building and so on. All these results will allow, in a further step, to setup a numerical model before the study of some real case.

Acknowledgements

We want to thanks the French Department of Environment and Durable Development for his research project DRS02 entrusted to the INERIS.

REFERENCES

Caudron M., Mathieu P., Emeriault F. and Al Heib M. 2003. Effondrement de cavités souterraines et interaction avec les ouvrages en surface, *Journées Nationales de la Géotechnique et de la Géologie pour l'Ingénieur*, juin 2003, 435-442.

Deck O., Al Heib M., and HOMAND F. (2003). Taking the soil-structure interaction into account in assessing the loading of a structure in a mining area. *Engineering Structure* 25:435-448.

Dehousse & Arnould (1971). Les modèles réduits de structure en Génie Civil. Paris: DUNOD, 183p.

Dolzhenko, N. & Mathieu P. (2001). Experimental modeling of urban underground works. Displacement measurement in a two-dimensionnal tunneling experiment. *Regional Conference on Geotechnical Aspects of Underground Construction in Soft Ground, Shangai, 2001*: 351-359.

Fine J., 1993. Le soutènement des galeries minières. *ARMINES, Centre de Géotechnique et d'exploitation du sous-sol* : 27-42.

IGC, 1999. Inspection Générale des Carrières : 222 ans de gestion de l'après carrière. *Annales des Mines. Janvier 1999 (*13): 31-37.

Lake L.M., Rankin W.J. and Hawley J; (1992). Prediction and effects of ground movements caused by tunnelling in soft ground beneath urban areas. *CIRIA funders report CP/5* 129p.

Nakai T., Xu L. and Yamazaki H. (1997). 3d and 2d model tests and numerical analyses of settlements and earth pressures due to tunnel excavation. *Soils and Foundations*, 37: 31-42.

Shashin H.M., Nakai T., Masaya H., Tomoki K. and Takashi S. (2004). Influence of surface loads and construction sequence on ground response due to tunneling. *Soils and Foundations*, 44(2): 71-84.

Touchal S., Morestin, F. and Brunet M. (1997). Mise au point d'une nouvelle méthode de mesure de champs de déformations par corrélation directe d'images numériques, *European Journal of Mechanical Engineering, BSMEE N°4*, 42:197-204.

Vachat JC., 1982. Les désordres survenants dans les carrières de la région parisienne. Etude théorique et pratique de l'évolution des fontis. *Mémoire présenté au conservatoire nationale des arts et métiers*, Paris.

White D., Take W. and Bolton M. (2003). Soil deformation measurement using particle image velocimetry (PIV) and photogrammetry. *Geotechnique*, 53:619-631.